Selective Growth of Al_2O_3 on Size-Selected Platinum Clusters by Atomic Layer Deposition

Timothy J. Gorey,[a] Yang Dai,[a] Scott L. Anderson[a]*

Sungsik Lee,[b] Sungwon Lee,[b] Soenke Seifert,[b] and Randall E. Winans[b]*

[a]Chemistry Department, University of Utah, 315 S. 1400 E., Salt Lake City, UT 84112

[b]X-ray Science Division, Argonne National Laboratory, 9700 South Cass Ave, Argonne, IL 60439

[*] Senior author

Corresponding Author: Scott L. Anderson, anderson@chem.utah.edu

ABSTRACT

In heterogeneous catalysis, atomic layer deposition (ALD) has been developed as a tool to stabilize and reduce carbon deposition on supported nanoparticles. Here, we discuss use of high vacuum ALD to deposit alumina films on size-selected, sub-nanometer Pt/SiO_2 model catalysts. Mass-selected Pt_{24} clusters were deposited on oxidized Si(100), to form model Pt_{24}/SiO_2 catalysts with particles shown to be just under 1 nm, with multilayer three dimensional structure. Alternating exposures to trimethyl-aluminum and water vapor in an ultra-high vacuum chamber were used to grow alumina on the samples without exposing them to air. The samples were probed *in situ* using X-ray photoelectron spectroscopy (XPS), low-energy ion scattering spectroscopy (ISS), and CO temperature-programmed desorption (TPD). Additional samples were prepared for *ex situ* experiments using grazing incidence small angle x-ray scattering spectroscopy (GISAXS). Alumina growth is found to initiate at least 60 times more efficiently at the Pt_{24} cluster sites, compared to bare SiO_2/Si, with a single ALD cycle depositing a full alumina layer on top of the clusters, with substantial additional alumina growth initiating on SiO_2 sites surrounding the clusters. As a result, the clusters were completely passivated, with no exposed Pt binding sites.

1. Introduction

Activity, selectivity, and stability are three important performance metrics for catalysts. Simultaneous optimization of all three is difficult, but atomic layer deposition (ALD) over-coating of supported nanoparticle (NP) catalysts has been shown to be a valuable approach toward this goal.[1-6] ALD uses self-limiting reactions to deposit films with atomic level control over thickness and has been used to modify catalysts in several ways. If many (typically > 20) ALD cycles are applied to deposit a thick overcoat, catalytic activity is suppressed, because the NPs are inaccessible to reactants. However, subsequent heat treatment can form nano-pores in the overcoat that allow access to the NP surfaces.[1, 7] The porous ALD layer acts as a physical barrier to minimize NP sintering, and may also improve the selectivity of the catalysts by selective blocking of low-coordination sites on the NPs. For example, ALD over-coated Pd NPs were used for oxidative dehydrogenation of ethane. With 45 cycles of Al_2O_3 ALD forming a ~7.7 nm thick layer on 2.8 nm Pd NPs, the heat-treated catalysts gave a 23% yield of the desired ethylene product, in contrast to 1.9% for the uncoated Pd NPs. The over-coated Pd NPs were also more stable under reaction conditions, with slower deactivation from coke formation and particle sintering. [1]

ALD can also be used to partially overcoat catalysts by applying fewer cycles, leading to a discontinuous film on the NPs and surfaces, which may block certain sites while leaving others accessible.[5] For example, Pd NPs (1 – 2 nm in diameter) were found to exhibit improved sintering resistance during methanol decomposition when over-coated by fewer than 16 cycles of Al_2O_3 ALD.[2] The active sites for this reaction, i.e., Pd(111) facets, were still accessible for methanol conversion, while low-coordination sites were preferentially blocked by the ALD overcoat. Because low-coordination surface sites are less stable than facet sites, they contribute

significantly to sintering. [8, 9] and may also be responsible for unwanted side reactions. The selective decoration of low-coordination surface sites by ALD was further confirmed using infrared spectroscopy.[10, 11] It was reported that 4 cycles of Al_2O_3 ALD over-coating, giving average thickness of 0.4 nm, effectively inhibits aggregation of Au particles (3 ± 0.4 nm in diameter),[10] however, in this case the overcoated NPs also lost much of their activity for CO oxidation. Activity recovered after calcination at high temperature, presumably due to re-exposure of active sites to the surface. In addition, ALD has been used to deposit a few layers of oxide on catalyst supports, such that subsequently deposited sub-nanometer particles were less susceptible to sintering under reaction conditions. [12, 13]

A trend in catalysis is use of smaller catalytic centers, including single-atom catalysts, where most or all of the metal is present as isolated atoms or small clusters. [14-16] By definition, such metal centers have low metal-metal coordination, raising the question of whether such centers can be stabilized or modified by ALD over-coating, without blocking metal binding sites entirely. Some studies have been successful. For example, tin oxide ALD was applied to Al_2O_3 membranes with Pt clusters deposited, reportedly resulting in SnO_x deposition on the alumina support, surrounding the clusters. SnO_x overcoating resulted in an increase in the selectivity for oxidative dehydrogenation of propane to propylene.[15] Another example of ALD overcoating was to deposit ~2 ML of alumina via ALD on Au clusters supported on a 3 ML ALD alumina film. The alumina overcoat served as an additional layer surrounding the clusters, preventing them from diffusing on the surface.[16]

Here, we present a study of alumina ALD on size-selected Pt_{24} clusters deposited on oxidized silicon (SiO_2/Si(100)) supports. These clusters were shown to remain intact, with minimal sintering/agglomeration at temperatures up to ~100 °C, and to remain un-oxidized after

air exposure. [17] The ALD process was studied by characterizing the samples, with and without ALD, using X-ray photoelectron spectroscopy (XPS) to probe electronic properties, grazing incidence small angle X-ray scattering (GISAXS) and low energy He^+ ion scattering (ISS) to probe morphology, and CO temperature-programmed desorption (TPD) to probe the accessibility of Pt surface sites. Alumina growth is shown to initiate selectively on the Pt_{24} clusters, hundreds of times more efficiently than on the SiO_2 support. The alumina blocks all CO binding sites, even for a single cycle of ALD that deposits less than 0.02 nm-equivalent of alumina (< 0.1 monolayer). While this particular example is probably not useful catalytically, we have been able to use the very high selectivity for ALD on sub-nano clusters as a method to alloy Pt clusters with boron[18, 19] or tin.[20]

2. Experimental

2.1 Preparation of Supported Size-Selected Pt Clusters

Model sub-nano $Pt_n/SiO_2/Si$ catalysts were prepared by depositing mass-selected Pt_n clusters on oxidized Si(100) substrates, using a cluster deposition instrument that has been described in detail elsewhere.[17] Briefly, the instrument has a multi-chamber UHV section equipped with stations for sample cleaning and annealing, cluster deposition, X-ray and UV photoelectron spectroscopy (XPS, UPS), low-energy ion scattering spectroscopy (ISS), and temperature-programmed desorption (TPD). Samples are positioned at each station using a manipulator where temperature can be controlled from ~150 to 2200 K. The samples can also be transferred off the manipulator into a separate UHV sample preparation ("prep") chamber which is equipped for gas dosing and mass spectrometry, thus allowing ALD to be performed on samples with no air exposure, while also minimizing contamination of the main UHV section by ALD reactants.

The system also has a load-lock chamber attached to the prep chamber, allowing facile exchange of samples.

A Pt_n^+ beam was generated by laser vaporization of a Pt target in a pulsed He flow. Cationic clusters were collected, deflected to eliminate neutrals, and guided by a series of radio-frequency quadrupole ion guides through six stages of differential pumping, undergoing mass selection by a quadrupole mass filter mid-way along the beam line. The final ion guide extends into the UHV system, terminating at a 2 mm diameter defining aperture. During deposition, substrates were positioned ~0.5 mm behind the 2 mm aperture. The deposition energy of the Pt_n clusters was calibrated by retarding potential analysis of the beam on the sample, and all of the samples used in these experiments were prepared with deposition energy of 1 eV/atom. Deposition was monitored via the Pt_n^+ neutralization current on the sample, and for all samples, deposition was stopped at a coverage of 1.50×10^{14} Pt atoms/cm^2, corresponding to ~10% of a close-packed Pt monolayer. For X-ray scattering experiments, samples were prepared by depositing four cluster spots in a row, to better overlap the footprint of the grazing incidence x-ray beam on the sample.

The Pt_n^+ were deposited on disposable SiO_2 substrates, prepared by dicing an oxidized Si(100) wafer into 10 × 14 mm pieces, using n-doped Si to give sufficient conductivity to eliminate charging during deposition and analysis. The SiO_2 substrates were clipped to a tantalum backing plate which was supported on tantalum heating wires that attached to a transferrable copper sample holder. A C-type thermocouple was spot welded to the backing plate for temperature measurement. The SiO_2 substrates were cleaned by heating to 800 K in UHV for 20 min prior to cluster deposition, such that no contamination is detected by XPS.

2.2 High Vacuum Al_2O_3 Atomic Layer Deposition (ALD)

Because our interest is in fundamental interactions of small clusters with the ALD reactants, we wanted to avoid complications from adventitious adsorbates that are inevitable when samples are transferred to an external ALD system. Therefore, ALD was carried out in the UHV system, by transferring samples into the prep chamber, onto a heating stage (300 – 1200 K) equipped with gas inlets for ALD, a sputter gun, and a residual gas analyzer (RGA - SRS 200) to monitor gases above the sample. The prep chamber base pressure (~8 x 10^{-10} Torr) was somewhat elevated due to frequent exposure to the ALD reactants, therefore it was kept isolated from the rest of the UHV system by a valve that was opened only for sample transfer.

Trimethylaluminum (TMA, Sigma-Aldrich, 97%) and deionized water were used as ALD reactants. Because the gas flows are small when doing ALD at high vacuum, accurate measurement and control of the sample exposures requires purification of the TMA reactant to remove methane present in the TMA cylinder headspace. A short section of the ~1 mm inside-diameter gas line was evacuated, and then cooled by a dry ice/ethanol bath. A small amount of gas from the TMA cylinder headspace was then passed through the cold section to condense the TMA, allowing CH_4 or any other volatiles to pump away. The line was then thawed to generate purified TMA vapor. With this procedure, the RGA showed no significant species other than TMA entering the UHV system during the TMA doses.

To reduce the exposure of the vacuum system to TMA and water, both reactants were delivered to the sample using separate dosing tubes terminating ~0.5 cm above the sample, with flows controlled by UHV-compatible leak valves. Pressures given below are the chamber background pressures measured with an ionization gauge, and we estimate that the local pressures at the sample surface were ~3 times higher.

Alumina growth by ALD involves repeated cycles of the following pair of reactions (* denotes surface species):

$$Al - OH^* + Al(CH_3)_3 \rightarrow Al - O - Al(CH_3)_2^* + CH_4 \quad (1)$$

$$Al - CH_3^* + H_2O \rightarrow Al - OH^* + CH_4. \quad (2)$$

Starting with $Pt_{24}/SiO_2/Si$, the process was initiated by first dosing the surface with water to hydroxylate reactive sites on the surface, and then repeated cycles of reactions one and two were carried out. Ott et al.[21] used ellipsometry to characterize the ALD growth rate of alumina on oxidized Si(100) at mTorr pressures, observing the most efficient growth at 450 K. In addition, incorporation of unreacted organic groups into the film increased at lower temperatures. We previously used grazing-incidence small angle X-ray scattering (GISAXS) to show that $Pt_{24}/SiO_2/Si$ was stable with respect to sintering up to 373 K, but that the particle size distribution (PSD) began to broaden and shift to larger diameter at higher temperatures.[17] Here, ALD was performed for some samples at room temperature, where sintering should be minimal, but other experiments were done at 423 K sample temperature, chosen as a compromise between efficient ALD film growth and cluster thermal stability.

Unless stated otherwise, the protocol was as follows: water was first dosed to an ionization gauge pressure of 2.0 x 10^{-6} Torr for 150 s, followed by 90 s of evacuation. TMA was then dosed, also at 2.0 x 10^{-6} Torr pressure for 150 s, followed by another 90 s of evacuation. For a single cycle of ALD, the process was completed by a final water dose at 2.0 x 10^{-6} Torr for 300 s, in an attempt to fully react all the TMA adsorbed on the sample and on other surfaces in the UHV system. For multiple cycles, pairs of 150 s water and TMA exposures were repeated, again terminating with a final 300 s water exposure. Dosing was monitored using the RGA to measure

intensities for mass 16, due primarily to CH_4 produced in the ALD reactions, and mass 57, which is characteristic of unreacted TMA.

To calculate the actual reactant doses at the sample position, we must correct for both the 3x pressure increase due to use of the dosing tubes, and the sensitivity of the ionization gauge to water and TMA. For water this was done using the manufacturer-reported sensitivity factor (~1), and for TMA, we estimated the sensitivity factor (~5) from the ratio of the 70 eV electron impact ionization cross sections for TMA[22] and for N_2.[23] After both corrections, the water dose is 900 L, the TMA dose 180 L, and the final water dose is 1800 L. Select experiments were also carried out at higher water and TMA doses, to verify that the protocol discussed above is sufficient to saturate the growth process (see below and the Supplementary Information).

2.3 In Situ Sample Characterization

Al Kα XPS, was done immediately following ALD, without air exposure to the sample, allowing us to measure the Al_2O_3 growth rate, and probe the electronic properties of the Pt_{24} clusters before and after ALD over-coating. The alumina growth rate averaged over the surface (i.e., on both Pt and SiO_2 sites) was determined from the ratio of Al 2p and Si 2p intensities, measured by XPS and modeled as described below. XP spectra were collected for both blank SiO_2 and Pt_n/SiO_2 samples to separate the growth on Pt cluster vs. SiO_2 sites. To monitor the alumina thickness deposited on top of Pt clusters, the attenuation of the Pt 4f intensity by ALD was used. Each experiment was done on a separately prepared sample in order to eliminate any effects of X-ray exposure.

ISS was done by scattering 1 keV He^+ from samples, providing insight into the morphology of as-prepared $Pt_{24}/SiO_2/Si$ and the effects of ALD over-coating. He^+ was incident on the sample at 45° at a beam current of either 3.0 μA (high flux) or 0.1 μA (low flux), with a ~7 mm diameter

beam spot that is substantially larger than the 2 mm diameter cluster spot (area ratio ~5.5). He^+ scattered along the surface normal was analyzed with a hemispherical energy analyzer. Each sample was probed by a series of ISS measurements to observe how signals change as material is slowly sputtered by the 1 keV He^+ beam. ISS experiments were done on separately prepared samples to avoid beam damage effects.

Because CO binds strongly to Pt, but not to SiO_2 or alumina, CO temperature-programmed desorption (TPD) was used to probe the number and binding energies of accessible Pt sites.[17] Samples were cooled to 180 K and exposed to 10 L of ^{13}CO, which is in excess of the saturation dose.[24, 25] The 180 K dose temperature was chosen to minimize CO adsorption on the SiO_2 support. The sample was then positioned 0.5 mm away from the 3 mm diameter aperture in a skimmer cone that separates the main UHV chamber from a separately pumped chamber housing a quadrupole mass spectrometer. The sample temperature was ramped at 3 K/s to 600 K, while monitoring signals for ^{13}CO, ^{12}CO, CO_2, $^{18}H_2O$, and $^{16}CH_4$. Three sequential CO TPD runs were carried out on each sample, to allow observation of changes in the number and energetics of CO binding sites induced by CO exposure and sample heating.

The absolute detection efficiency of the TPD mass spectrometer was calibrated daily, allowing the $^{13}CO^+$ ion signals observed during TPD to be converted to absolute numbers of desorbing CO molecules. For this calibration, 2.0×10^{-8} Torr of ^{13}CO was leaked into the main chamber, as measured with a nude ion gauge, corrected using the sensitivity factor reported by the manufacturer. This produces a well-defined flux of ^{13}CO through the skimmer aperture into the mass spectrometer ion source, which can be compared to the simultaneously measured $^{13}CO^+$ signal. During TPD, CO desorbs only from the 2 mm diameter cluster spot, whereas during calibration, the CO flux is determined by the 3 mm diameter skimmer aperture, and this factor is

included in the calibration. The angular and velocity distributions of molecules desorbing during TPD differ from those of CO effusing into the mass spectrometer during calibration, which will have some effect on the ionization efficiency. We have also calibrated using CO desorption from single crystals with known CO coverage, with similar results. [26] Nonetheless, we only claim absolute calibration to within ~50 %.

2.4 Ex Situ Sample Characterization

To determine changes in surface order by ALD deposition, a clean Pt_{24}/SiO_2 sample and Pt_{24}/SiO_2 with 1 cycle of ALD overcoat were prepared for *ex situ* GISAXS characterization. The samples were transferred out of the UHV system and placed in a custom-made sample container in air, then shipped to Argonne National Laboratory (ANL). The ALD treated sample was prepared at room temperature prior to shipment to ANL. When samples were received at Argonne, they were taken out of the housing and transferred to a Kapton-sealed cell in an N_2 glove box, then moved to the beamline for x-ray studies.

GISAXS experiments were performed using an instrument developed at Sector 12-ID-C at the Advanced Photon Source.[27] The X-ray beam, tuned to the Pt L_3 absorption edge, was scattered off the sample at grazing incidence, at the critical angle (α_c= 0.15°) of the substrate. A 1024 × 1024 pixel two-dimensional CCD detector designed and built at the APS was used for recording the GISAXS images from the sample. Measurements were made at incident energy of 18 keV with a scattering vector (q) range of 0.008 – 0.5 $Å^{-1}$, and the scattering vector was calibrated using a silver behenate sample. The size distributions of scatterers present on the sample surfaces were determined by fitting the GISAXS data using the Modeling II tool in the Irena package. [28] Note that samples were prepared by random deposition of clusters, with

average inter-cluster separation for Pt_{24} of ~5 nm, and for the oxidized Si substrate, we do not expect any substrate-driven ordering of the clusters.

3. Results

*3.1 Characterization of Al_2O_3 Growth Rate by High Vacuum ALD*The ALD growth rate on Pt-free SiO_2/Si was characterized by XPS. **Fig. 1** shows the results for growth at a sample temperature of 423 K and using reactant doses as described above. In **Fig. 1a**, Al 2p region scans were plotted after repeated ALD iterations. The Al 2p binding energy (BE) was 75.3 eV, which is in the range expected for oxidized Al. There was a clear increase in Al 2p intensity with number of ALD cycles, showing that each iteration of TMA and H_2O exposure resulted in additional deposition of alumina. Deposited alumina was quantified by modeling the ratio of the integrated intensities for the Al 2p and Si 2p peaks. Photoemission cross-sections and asymmetry parameters from Yeh and Lindau,[29] and effective attenuation

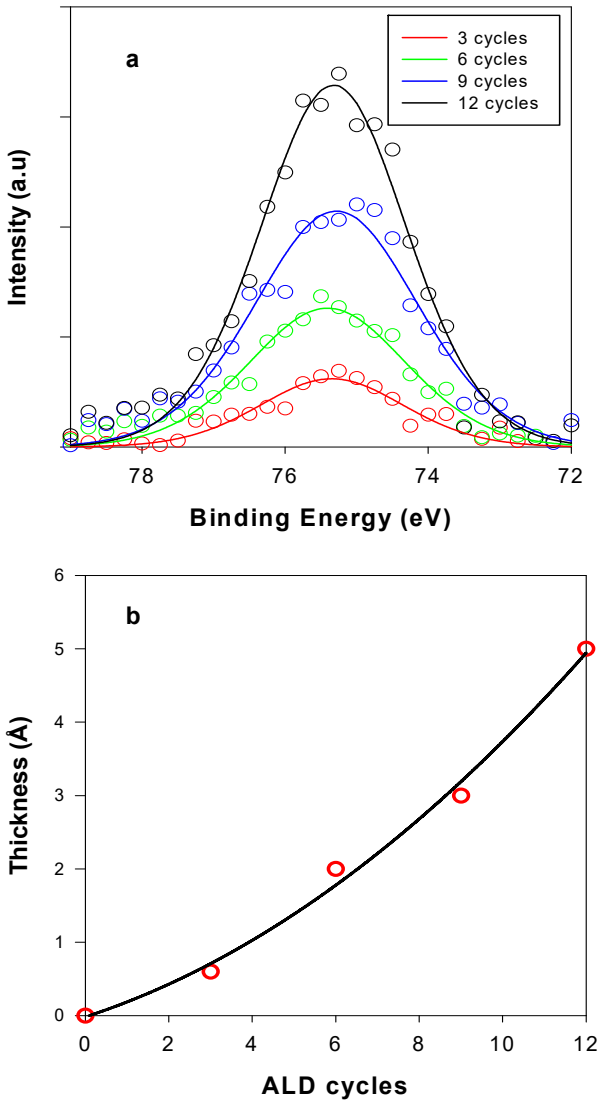

Fig. 1. The growth rate calibration of alumina ALD on a clean silica substrate at the surface temperature of 423 K. (a) XP spectra of Al 2p (b) Calculated thickness of Al_2O_3 as a function of ALD cycles.

lengths (EAL) calculated using the NIST EAL Database version 1.3,[30] were used to simulate the signals expected from a variable thickness of Al_2O_3 on SiO_2/Si.[24] A total of 12 ALD cycles were performed, with deposited Al_2O_3 quantified every three cycles. Thickness results are shown in **Fig. 1b**. The average growth rate over 12 cycles was ~0.4 Å per cycle, but the growth rate clearly accelerated, from ~0.2 Å/cycle averaged over the first three cycles, to ~0.67 Å/cycle for the last three cycles. The Al XPS intensity is too low during the initial cycles to allow details of the growth initiation to be extracted, and the data have fit to an exponential, chosen simply as a convenient functional form. Note that for a large enough number cycles, the growth is expected to become linear. For example, Ott *et al.*[21]reported linear growth of 1.1 Å/cycle for alumina ALD on oxidized SiO_2/Si(100) (i.e., the same substrate we used), under viscous flow ALD conditions, and similar results were reported by Wind and George[31] for Al_2O_3 growth on a quartz crystal microbalance.

Fig. 1 suggests that with enough cycles, the growth rate in our experiment would accelerate to be similar to the rates observed in the higher pressure ALD reactors, but the initial rate is ~5 times lower. One obvious possibility might be that our reactant doses (900 L H_2O; 180 L TMA; 1800 L H_2O) are too small to saturate the available growth sites, and to test this hypothesis, we also measured the growth for reactant doses 25 times higher, with water dosed at 22,500 L and TMA dosed at 4500 L. Shown in **Fig. S1**, the difference in growth rate was negligible, i.e., the gas dose was not the limiting factor, even at the lower dose.

The alumina growth rate was also measured for ALD performed at room temperature, using the lower of the two doses of TMA (180 L) and water (900 L before TMA, 1800 L after TMA). Shown in **Fig. S2**, the average growth rate was 0.92 Å/cycle, in other words, about twice as large as for the same reactant dose at 423 K. This result may seem surprising, but as shown below, it

probably reflects incomplete reaction during growth, resulting in substantial incorporation of organic fragments and hydroxyl groups into the alumina layer.

There are several differences between our experiment and that of Ott et al. which presumably explain our ~5 times lower initial growth rate. Our growth temperature (423 K) is slightly lower than the optimum temperature found by Ott et al. (450 K), but based on the weak temperature-dependence, we expect the small difference in temperature to result in only a few percent change in growth rate. Instead, our slower initial growth rate is attributed to the density of ALD initiation binding sites. In the Ott et al. work, the oxidized Si sample was pretreated with a H_2O plasma prior to ALD for sample cleaning, but this also presumably a high density of hydroxyls on the surface, serving as ALD initiation sites. In our experiment, the oxidized Si substrate was heated to 800 K in UHV for 20 min for sample cleaning, which should desorb most hydroxyls (and other contaminants) that might have been present from air exposure. The surface was dosed with water at the beginning of ALD, but the slow initial growth rate implies that the density of ALD initiation sites (e.g. hydroxyls) created by simple water exposure is small, suggesting that water reacted with the SiO_2/Si surface only at a small number of defect sites. This conclusion is supported by consideration of the growth rates in terms of the fraction of an alumina monolayer that is deposited *per* ALD cycle. Ott et al. estimated the thickness of one ALD alumina layer to be 3.64 Å, i.e., even their best ALD growth rate (~1.1 Å/cycle) corresponded to less than 1/3rd of a layer. Our initial growth rate of 0.2 Å/cycle corresponds to ~5 % of a monolayer, which is a plausible value for the density of defect sites on the oxidized Si surface. The increase in growth rate during subsequent ALD cycles suggests that alumina islands, initially initiated on only about ~5 % of the surface, spread laterally as they grow, allowing ALD to proceed on an increasing fraction of the surface.

Both the temperature and dose dependence of alumina ALD have been studied previously. Ott et al.[21] used ellipsometry to characterize the alumina ALD growth rate on oxidized Si(100) (i.e., the same substrate used here) at substrate temperatures ranging from 350 to 650 K, with reactants dosed at ~20 mTorr. For 250 ALD cycles, the fastest growth rate was observed at 450 K (~1.1 Å/cycle), with thickness found to be linear with the number of ALD cycles. In this regime, the growth rate was only weakly dependent on temperatures between 350 and 500 K. For example, at 400 K, the rate was ~1 Å/cycle. Similar behavior was observed by Elam *et al.* in a viscous flow reactor.[32] Our observation of higher growth at room temperature is consistent with Ott et al., [21] who used IR spectroscopy to look at CH and OH stretch vibrations associated with organics and hydroxyls incorporated in alumina films grown by ALD and observed increasing intensity with decreasing growth temperature. Also addressing the lower-temperature regime, Gröner et al. measured the temperature-dependence of Al_2O_3 growth on SiO_2/ Si(100) between 375 and 450 K on. The highest growth rate achieved was ~1.3 Å/cycle at a temperature of ~400 K, but the growth rate was only weakly temperature dependent in this range, with a minimum of ~1.1 Å/cycle at 375 K.[33] Other studies of alumina grown on silica surfaces have used temperatures up to 923 K.[21, 34-37]

As noted, our typical TMA and water doses were ~180 L/cycle, and we found that increasing our doses by a factor of 25 (to ~4,500 L) resulted in no significant increase in alumina deposition/cycle, i.e., growth was saturated even at the lower dose. Note, however, that even our largest reactant dose was far below those used in most studies. For example, Wind and George measured 400 K alumina ALD deposition onto a quartz crystal microbalance (QCM), monitoring growth as a function of exposure.[31] They reported that ALD was already saturated at their lowest TMA dose (260,000 L), but noted that growth was not completely self-limiting (i.e., there

was a small amount of additional growth at higher doses). Lownsbury et al.[35] examined alumina growth on several substrates (not including SiO_2), using a protocol in which TMA was applied as 15 pulses of ~0.17 Torr·s each (170,000 L/pulse, ~2,550,000 L total), followed by similar multiple pulse water exposures. Reaction was studied calorimetrically and growth rates were measured using a QCM. Under these conditions, a single TMA pulse (i.e., 170,000 L) was sufficient to nearly saturate growth. Thus, our observation that 180 L TMA and water doses are sufficient to saturate growth under high vacuum conditions, is consistent with previous studies, but explores a very different dose and gas flow regime (molecular vs. viscous flow).

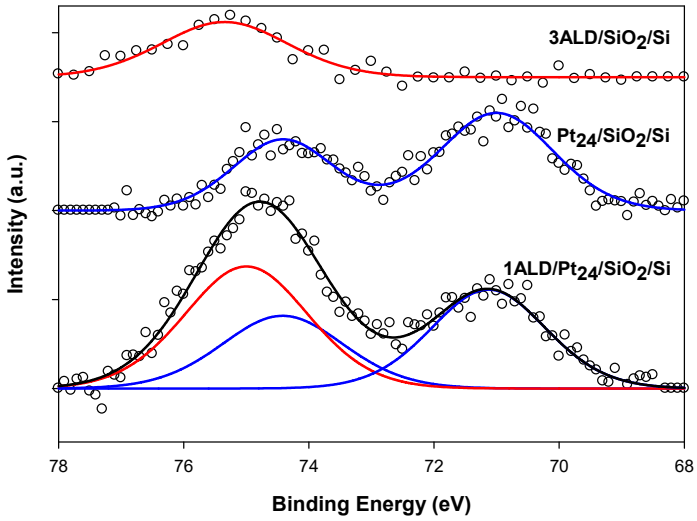

Fig. 2. XPS of the Pt 4f and Al 2p region. Top: spectrum for a SiO_2/Si substrate after three 3 ALD cycles (423 K). Middle: Spectrum of as-deposited $Pt_{24}/SiO_2/Si$. Bottom: Spectrum for $Pt_{24}/SiO_2/Si$ after one ALD cycle (423 K), with fits showing contributions from Al 2p (red) and Pt 4f (blue).

From the perspective of understanding the interaction of ALD reagents with the deposited Pt_n clusters, the low reactivity of the SiO_2 substrate is advantageous, allowing us to observe how the presence of even a small coverage of Pt_{24} affects the area-averaged growth rate. **Fig. 2** shows that the presence of 0.1 ML of Pt_{24} indeed results in a substantial increase in growth rate. Al 2p and Pt 4f XPS signals are compared for samples with and without Pt_{24}, with and without ALD.

The top spectrum shows the region of the Al 2p and Pt 4f peaks for a Pt-free SiO_2/Si sample exposed to *three ALD* cycles, resulting in a small Al 2p peak at ~75.25 eV. The middle spectrum is for as-deposited $Pt_{24}/SiO_2/Si$, without any ALD. Signal is seen for the Pt $4f_{7/2}$ and $4f_{5/2}$ peaks at ~71.0 and ~74.4 eV, respectively. As shown in the bottom spectrum, a *single ALD cycle* on $Pt_{24}/SiO_2/Si$ has little effect on the Pt $4f_{7/2}$ peak, but results in a large peak at ~75 eV due to overlapping contributions from Al 2p and Pt $4f_{5/2}$. Because the Pt $4f_{7/2}$ and $4f_{5/2}$ peaks are in a fixed, 4:3 intensity ratio, it is straightforward to separate the Al 2p and Pt $4f_{5/2}$ contributions, as shown by the fits.

The fitted Al 2p feature for a single ALD cycle on $Pt_{24}/SiO_2/Si$ is a peak at 75.0 eV, with integrated intensity ~2.1 times greater than the Al 2p intensity following three cycles on SiO_2/Si, i.e., there is roughly six times as much Al deposition *per* ALD cycle when Pt_{24} is present. In fact, however, the enhancement of the growth rate from the presence of Pt_{24} is much greater than six fold, because our XPS analysis area is >10 times the area of the ~2 mm diameter cluster spot, and even within the cluster spot Pt_{24} only occupies ~10% of the surface area.

To estimate the growth rate associated with the Pt clusters more quantitatively, the Al 2p intensity in the top spectrum (3 ALD/SiO_2/Si) was divided by three to approximate the intensity expected from a single ALD cycle on the Pt-free substrate. This was then subtracted from the bottom spectrum (1 ALD/$Pt_{24}/SiO_2/Si$), to approximately subtract the contribution from ALD on the SiO_2/Si substrate, giving an estimate of the Al 2p signal associated with growth on the clusters. Because both the Al and Pt are present in a thin deposit on top of the SiO_2/Si substrate, attenuation of Al and Pt photoelectrons by inelastic scattering can be neglected to a good approximation (the effective attenuation lengths would both be in the ~27 Å range[30]). Therefore, the Al to Pt ratio can be estimated as $X_{Al}/X_{Pt} = I_{Al}/I_{Pt} \cdot \sigma_{Pt}/\sigma_{Al}$, where X_{Al}/X_{Pt} is the Al

to Pt coverage ratio, I_{Al}/I_{Pt} is the measured Al 2p/Pt 4f ratio, and σ_{Pt}/σ_{Al} is the ratio of the Al 2p and Pt 4f photoemission cross sections, taken from the work of Yeh and Lindau.[29] The σ_{Pt}/σ_{Al} ratio is ~31, and as a result, the ratio X_{Al}/X_{Pt} is ~19.8, i.e., a total of ~20 aluminum atoms are deposited *per* Pt atom. This increase in total alumina deposition in association with Pt clusters is *far larger* than can be explained by a self-limiting ALD process, even if alumina growth initiates on Pt sites with unit efficiency.

The attenuation of the Pt $4f_{7/2}$ peak after one cycle of ALD (i.e., comparing the bottom and middle spectra in Fig. 2) provides a complementary measure of the amount of alumina deposited, however, the attenuation is sensitive only to alumina *on top of the Pt* clusters. The attenuation from a single ALD cycle is 10.0 %, and the effective attenuation length for Pt 4f photoelectrons in alumina is ~27 Å,[30] thus from Beer's law the alumina thickness on top of the Pt clusters is ~2.9 Å. This is roughly what would be expected for a single alumina layer on top of the Pt clusters, however, the corresponding amount of Al is far less than is implied by the ~20:1 Al-to-Pt stoichiometry calculated from the Al 2p-to-Pt 4f XPS intensity ratio.

The fitted binding energy for Al 2p in the overcoated sample is ~75 eV, which is at the high end of the range of BEs reported for bulk Al_2O_3 or aluminum hydroxides, and at the low end of BEs reported for alumina films on aluminum.[38] Furthermore, there is also a report that the Al 2p BE for TMA on silver is 75.0 eV,[39] thus, the Al 2p BE is consistent with aluminum an oxidized state, but does not reveal the film composition.

3.2 Characterization by GISAXS.

GISAXS was used to characterize the effects of ALD on the sample morphology. These experiments required the samples to be transferred to the APS at ambient temperature, thus one question is whether the clusters remained intact during transfer. **Fig. 3a** compares the raw room temperature GISAXS data for SiO_2/Si with no clusters deposited ("SiO_2 blank"), for as-deposited, soft-landed Pt_{24}/SiO_2/Si, and for soft-landed Pt_{24}/SiO_2/Si with 1 cycle of room temperature alumina ALD carried out after cluster deposition. This set of samples was transferred to the APS in air, but studied in a flow of helium. Compared to the SiO_2/Si blank, Pt_{24} deposition results in additional scattering in the q range between 0.02 and 0.4 $Å^{-1}$. One room temperature ALD cycle results in a much larger increase in scattering signal over the entire q range studied.

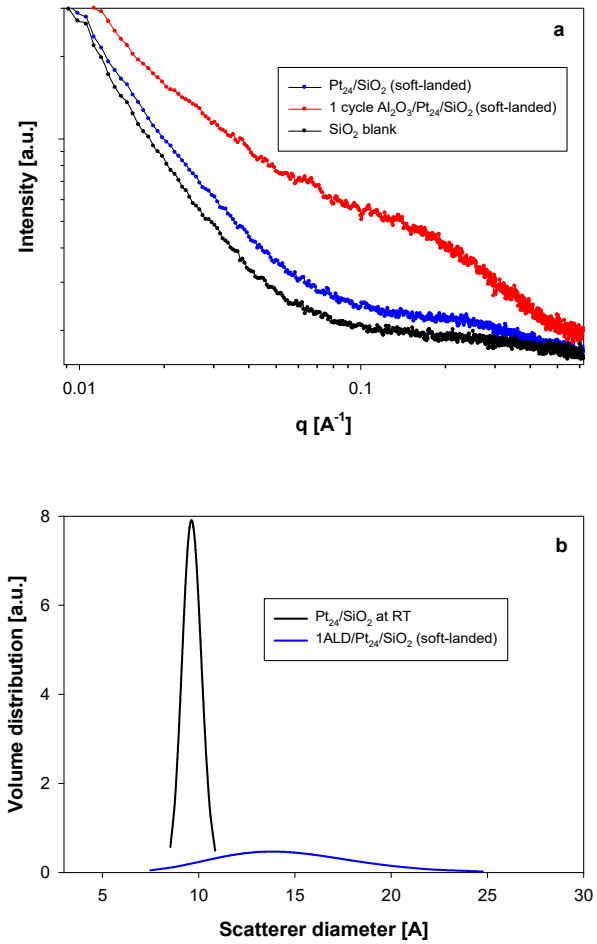

Fig. 3. GISAXS for soft-landed Pt_{24}/SiO_2/Si transferred in air, an ALD overcoated sample, and a clean blank SiO_2/Si sample. (a) Raw GISAXS scattering data (b) Fitted size distributions extracted by fitting the scattering data as in (a) for soft-landed Pt_{24}/SiO_2/Si, as well as soft-landed Pt_{24}/SiO_2/Si with 1 cycle of Al_2O_3 ALD overcoat.

After subtracting the scattering signal from the SiO_2/Si support, the GISAXS data can be fit to estimate the scatterer size distributions, which are shown in **Fig. 3b**. Because GISAXS was done at the Pt edge, it is sensitive to disorder associated with the Pt clusters. For as-deposited Pt_{24}, the scatterer size distribution extracted from the GISAXS data is narrow and peaked at 0.96 nm – about what would be expected for flattened 24 atom Pt islands on a surface (spherical Pt_{24} would be ~9 Å). The distribution observed after one cycle of room temperature ALD is much broader (FWHM ≈ 8.4 Å), and shifted to peak at ~14 Å. This large increase in the diameter of the Pt-associated scatterer distribution is consistent with the conclusion from XPS, that the presence of Pt clusters results in efficient alumina deposition on the clusters, but also catalyzes alumina deposition on the surrounding substrate.

For comparison, in a previous study,[17] we studied the effects of annealing $Pt_{24}/SiO_2/Si$ to various temperatures. Temperatures up to 372 K resulted in no significant change in the GISAXS of as-deposited $Pt_{24}/SiO_2/Si$, i.e., no significant sintering occurred. For temperatures of 423 K or higher, sintering was evident in GISAXS, but for 423 K (the temperature used in many of the ALD experiments), the scatterer size distribution remained peaked near 10 Å, with a tail extending to larger sizes.[17, 40] The extent of broadening was smaller than that observed after a single cycle of room temperature ALD.

3.3 Morphology Characterization by ISS

Further evidence regarding the morphology of both the Pt_{24} clusters and the ALD alumina layer was obtained by probing samples with 1 keV He^+ ion scattering. As an example, **Fig. S3** shows a full survey ISS spectrum for soft-landed $Pt_{24}/SiO_2/Si$. The peaks result primarily from events where He^+ scatters from a single atom in the top-most layer of the sample, while multiple scattering and scattering from atoms below the surface layer contribute primarily to the weak,

featureless background at low E/E_0.[41] In **Fig. S3**, clear peaks are seen for O, Si, and Pt, as expected.

Fig. 4 shows how the Pt ISS signal evolves as the sample is exposed to the He^+ beam, which slowly removes atoms by sputtering. **Fig. 4a** shows select raw Pt ISS spectra. Note that in the first scan, only a small Pt signal is observed, consistent with the conclusion from XPS that ALD initiates efficiently on the clusters, leaving them with a ~2.9 Å thick AlO_x overlayer. This overlayer almost completely attenuates He^+ scattering signal from Pt due to a combination of shadowing, blocking, and low ion survival probability.[25] In the 2nd and 3rd scans, the Pt signal increases as the He^+ beam sputters atoms from the alumina overlayer. The final spectrum was

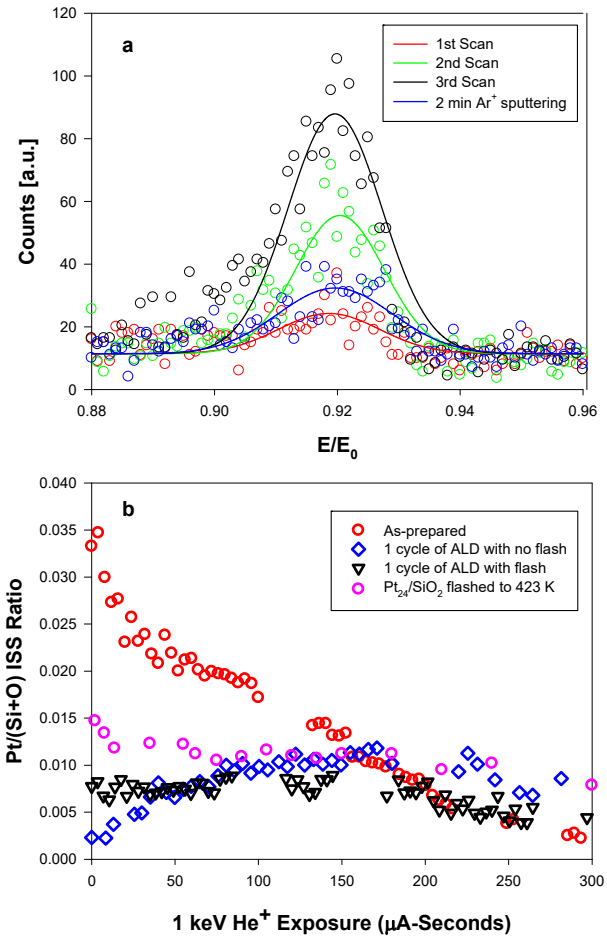

Fig. 4. Pt ISS results for (a) three consecutive high flux ISS scans and a final scan after 2 min of 1 keV Ar^+ sputtering on the sample 1ALD/$Pt_{24}/SiO_2/Si$, where ALD was performed at the substrate temperature of 423 K. (b) Normalized Pt ISS intensity for $Pt_{24}/SiO_2/Si$ (red), samples with 1 cycle of ALD overcoat with (black) or without (blue) flash post-treatment, and a sample annealed at 423 K in vacuum (pink).

for a sample with 2 minutes of Ar^+ sputtering. Because of its higher Z and scattering cross-section, Ar^+ sputters material much more rapidly than He^+, resulting in low signal due to most of the Pt having been sputtered away.

Fig. 4b shows the Pt signals as a function of He^+ exposure for samples with identical Pt_{24} coverage, but with various treatments applied prior to ISS analysis. To account for any day-to-day variations in the He^+ beam intensity, the signals were normalized to the sum of the Si, Al, and O signals. To allow measurements for smaller increments of He^+ exposure, most spectra were scanned only over the Pt region, with occasional full spectra to observe how the O, Si, and Al peaks evolved, resulting in the more widely spaced points.

For as-deposited, adsorbate-free $Pt_{24}/SiO_2/Si$, the Pt signal is initially high, decreasing monotonically with He^+ exposure as the Pt is sputtered away. For a $Pt_{24}/SiO_2/Si$ sample that was simply heated to 423 K in UHV, the initial Pt signal is ~50% lower, indicating that ~50% fewer of the Pt atoms were in the surface layer. Attenuation at this level could result from Pt_{24} sintering into larger, more multilayer clusters, or simply restructuring of initially flattened clusters into more three-dimensional structures. Previous GISAXS results for Pt_{24}/SiO_2 heated to 423 K are consistent with a modest degree of cluster sintering, as discussed above.[17] For the heated sample, the Pt signal also decreases monotonically with He^+ exposure, but more slowly than for the unheated sample. This behavior is also consistent with multilayer Pt clusters, where sputtering of surface layer Pt exposes additional underlying Pt.

When $Pt_{24}/SiO_2/Si$ was overcoated with 1 cycle of ALD at 423 K, the initial Pt ISS signal is attenuated by ~93% relative to as-deposited $Pt_{24,}$ and slowly *increases* during the initial ~200 μA·sec of He^+ exposure. This behavior shows that the Pt was covered by a layer of adsorbed material attenuating almost all Pt ISS signal, which recovered as the overlayer sputtered away. It

does not take much of an overlayer to substantially attenuate ISS from underlying atoms. For example, a coverage of ~0.8 CO molecules *per* surface Pd atoms was sufficient to attenuate Pd ISS signal from a Pd_{20}/TiO_2 sample by ~80%.[26] In that example, the Pd ISS signal recovery was about twice as fast as that observed here for 1 cycle of ALD alumina on Pt_{24}, however, sputter rates are strongly dependent on binding energy, and the CO binding energy is almost certainly lower than that of Al and O atoms in an alumina overlayer.

Note that if the overcoated sample was flashed to 600 K prior to ISS analysis, the initial attenuation of the Pt ISS signal was only ~80%, relative to as-deposited $Pt_{24}/SiO_2/Si$. In addition, rather than the Pt ISS intensity increasing initially, it was roughly constant during the first ~150 μA·sec of He^+ exposure. Constant signal implies that the rate at which Pt is exposed by sputtering of overlying adsorbates is matched by sputter loss of surface Pt. Additional insight into the effects of heating on the ALD-treated sample is obtained from the TPD experiments discussed below.

3.4 Temperature-Programmed Desorption (TPD)

CO TPD experiments were performed to probe several related issues: the density of accessible Pt binding sites on the samples, the presence of pyrolyzable organic material in the ALD alumina layer, and the CO sticking/desorption temperature dependence on both SiO_2 and Pt_{24}. CO was chosen as the probe because it binds strongly to small Pt clusters but not to oxide supports,[20, 24, 26, 42, 43] and thus provides insight into the effects of ALD overcoating on the number and energetics of accessible Pt sites. A series of sequential ^{13}CO TPD runs were made on samples in order to observe how the CO binding properties changed with heating. Before each TPD run, the samples were exposed to 10 L of ^{13}CO at 180 K, and then heated at 3 K/s

while monitoring species desorbing from the surface. The 180 K exposure temperature was chosen to minimize CO binding on the SiO_2 support, while saturating sites associated with Pt_n.[42]

Note that, unlike the XPS and ISS experiments, where the analysis area is significantly larger than the 2 mm diameter cluster spot, our TPD differential pumping cone has an aperture that is only 38% bigger than the cluster spot, and the sample is positioned close enough to the cone that little or no desorption from surfaces outside the aperture area is detected.

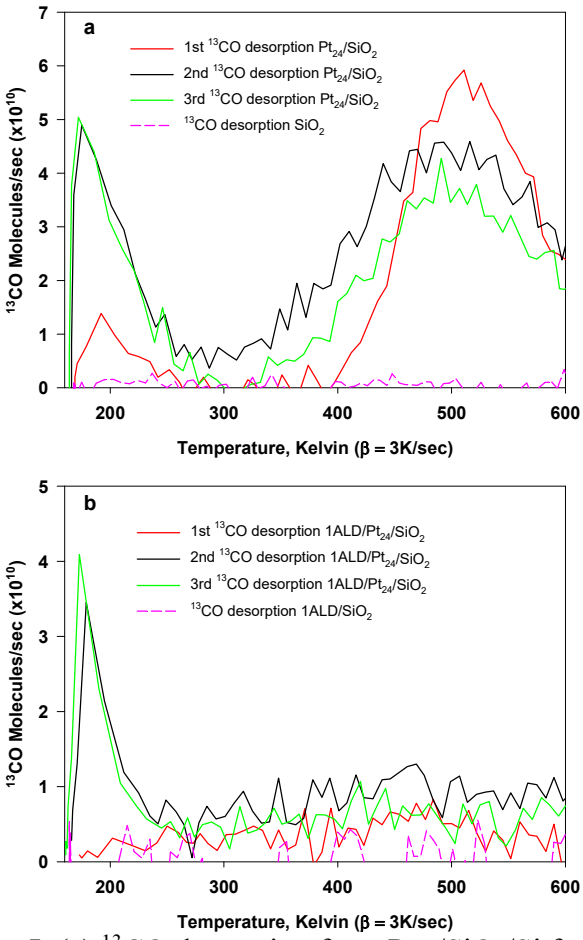

Fig. 5. (a) ^{13}CO desorption from $Pt_{24}/SiO_2/Si$ for three consecutive CO TPDs (solid), and a blank SiO_2/Si sample (dashed), after 10 L ^{13}CO exposure at 180 K. (b) ^{13}CO desorbing from $Pt_{24}/SiO_2/Si$ with 1 cycle of ALD overcoat for three consecutive CO TPDs (solid) and a blank SiO_2/Si sample with 1 cycle of ALD overcoat (dashed).

3.4.1 CO Desorption as a Probe of Pt Binding Sites

As shown in **Fig. 5a,** no ^{13}CO desorption was observed for a Pt-free SiO_2/Si sample (pink), indicating that CO does not bind to SiO_2/Si at 180 K. In the first TPD from $Pt_{24}/SiO_2/Si$ without ALD overcoating, there are two CO desorption features, peaking at ~190 K and ~510 K. Assuming 1st order desorption kinetics and a prefactor of 10^{14} sec^{-1},

Redhead analysis of the peak desorption temperatures gives desorption energies of roughly ~0.5 eV and ~1.5 eV for the two components.[44] In the second TPD run, the high-temperature feature broadened, and its peak shifted to ~490K, while the low temperature feature strengthened. There was little change in the third TPD run, apart from a slight decrease in the intensity of the high temperature feature. These features, and the effects of multiple TPD runs, are quite similar to what was observed in CO desorption from Pt_n ($1 \leq n \leq 18$) deposited on a ~3 nm thick alumina film grown on Re(0001).[42]

Fig. 5b shows ^{13}CO TPD data taken under identical conditions for samples that were exposed to 1 cycle of ALD alumina overcoating, prior to TPD analysis. Overcoating was done at 423 K with reactant exposures of 2 x 10^{-6} Torr for 150 s. For ALD-overcoated SiO_2/Si, no significant ^{13}CO desorption was observed, indicating that ALD on the SiO_2/Si support did not create any new CO binding sites stable at T > 180K. For the ALD-overcoated Pt_{24}/SiO_2/Si sample, the first TPD run also showed little CO desorption, indicating that the overcoated sample had few sites able to bind CO at the 180 K exposure temperature. In the second TPD run, a low temperature CO desorption feature was observed, with somewhat lower intensity and sharper temperature dependence than the low temperature feature observed for as-deposited Pt_{24}/SiO_2/Si. Desorption at higher temperatures remained suppressed, with no obvious peak. The third TPD showed similar results.

These results demonstrate that a single cycle of 423 K ALD alumina overcoating blocks or destabilizes CO binding sites associated with Pt_{24}, such that no adsorption occurs at 180 K. After the first TPD run, CO binding sites are again available, however, these are weak binding sites that desorb at low temperatures. The stronger, and catalytically more interesting binding

sites responsible for desorption around 500 K for bare Pt_n remain blocked even after repeated heating to 600 K.

The nature of the low temperature CO binding sites that reappear after annealing of the overcoated sample is not clear. As shown in **Fig. 5a**, there are CO binding sites associated with Pt in this temperature range. On the other hand, we have also observed CO desorption in this temperature range for defective alumina films grown on single crystal supports,[42, 45, 46] thus the sites exposed by annealing may simply be defects in the alumina.

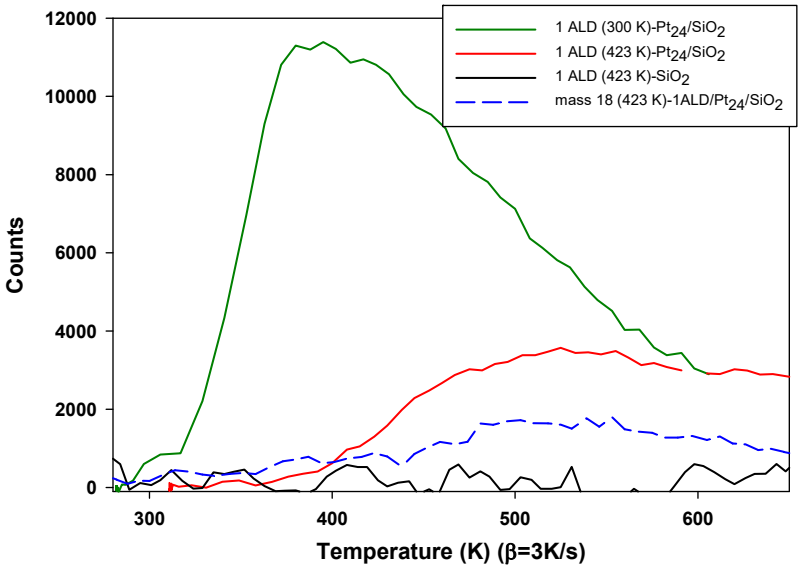

Fig. 6. Mass 16 TPD following a single alumina ALD cycle on $Pt_{24}/SiO_2/Si$ at either 300 K (green) or 423 K (red), and on SiO_2/Si at 423 K (blue). Mass 18 desorption from 423 K 1 ALD-Pt_{24}/SiO_2.

3.4.2 Desorption of Organics from the ALD Alumina Layer

The partial recovery of CO binding sites associated with overcoated Pt_{24} after 600 K heating, suggest that the alumina layer undergoes changes, and one obvious possibility is loss of unreacted organic moieties and water/hydroxyl incorporated during ALD. **Fig. 6** shows the mass 16 TPD signal recorded during the first CO TPD run on SiO_2/Si and $Pt_{24}/SiO_2/Si$ samples overcoated with one alumina ALD cycle. For $Pt_{24}/SiO_2/Si$, both 300 K and 423 K ALD

overcoating was examined. Mass 16 is the major peak in the EI mass spectrum of methane, and is also a significant peak for EI of TMA.

For the SiO_2/Si substrate with one 423 K ALD cycle, the mass 16 desorption signal is insignificant, as might be expected from the small Al XPS signal observed after ALD on the Pt-free SiO_2/Si substrate. XPS tells us that Al deposition is inefficient on the substrate, thus there is little organic material on the surface to desorb. The absence of water desorption (not shown) indicates that water adsorption on the substrate at 423 K during the final step in ALD, is also inefficient.

In contrast, after one cycle of 423 K ALD overcoating of Pt_{24}/SiO_2/Si, there is substantial mass 16 desorption starting at 400 K, peaking just above 500 K. There is also a broad water desorption feature, with similar temperature dependence. The fact that methane and water desorption start near 400 K reflects the 423 K ALD temperatures – any methane or water that could desorb at lower temperatures was lost during the ALD process. The apparently lower onset of water desorption probably is due to adsorption of weakly bound adventitious water (from the UHV background) as the sample was cooled to the TPD dose temperature.

Gow et al.[47] previously reported TPD of TMA adsorbed on clean Si(100). They identified two contributions to the mass 16 signal, including mass spectrometer cracking of TMA, or fragments thereof, desorbing in the 300 K - 600 K range, and ionization of methane desorbing in the 400 K - 800 K range. Given that our samples were exposed to large doses of water after TMA exposure, it is unlikely that intact TMA remains on the surface, but clearly there are organic moieties present, as well as unreacted hydroxyl groups and/or adsorbed water. **Fig. 6** shows that these can react, resulting in methane desorption, and that there also is recombinative desorption of water.

There is also the question of whether significant residual organic moieties remain after the first CO TPD. As shown in **Fig. S4 (top)** for the 300 K ALD-overcoated $Pt_{24}/SiO_2/Si$ sample, no significant mass 16 desorption was observed in the second CO TPD. This is not surprising – any water or methane that could form and desorb in the TPD temperature range would have been lost in the first TPD run. Similar results were observed for mass 16 desorption from 423 K ALD-overcoated $Pt_{24}/SiO2$ as shown in **Fig. S4 (bottom)**. For one cycle of 300 K ALD on $Pt_{24}/SiO_2/Si$, the mass 16 desorption starts just above 300 K, and peaks at ~380 K, with ~2.6 times as much integrated signal, compared to 423 K ALD. This observation is consistent with the results of Ott et al.,[21] who observed increased incorporation of organic moieties in ALD alumina films grown at lower temperatures. The choice of 423 K for ALD in the main set of experiments was driven by the conflicting desire to have as little organic contamination of the alumina as possible, while also minimizing thermal sintering of the Pt_{24}. As noted, 423 K is close to the 450 K optimum Al_2O_3 ALD growth temperature reported by Ott et al.[21]

4. Discussion

For the temperature range and dosage studied here, Pt binding sites show high propensity to initiate ALD, compared to clean, vacuum-annealed SiO_2, as shown by XPS, ISS, and attenuation of Pt binding sites for CO. One question is whether the loss of high temperature CO binding sites is entirely due to physical blocking of the sites by alumina, or if there are also effects on the Pt_{24} electronic structure. The XPS measurements provide evidence here. **Fig. 2** compares the Pt 4f XP spectra measured for $Pt_{24}/SiO_2/Si$, as-deposited in UHV and after 1 cycle of 423 K ALD overcoating. For the as-deposited sample, the Pt $4f_{7/2}$ binding energy (BE) is 71.0 eV, which is in the range reported for the Pt $4f_{7/2}$ BE for bulk Pt (70.9 eV to 71.3 eV, with an average of 71.2 eV).[38] As discussed elsewhere,[48-50] core level binding energies for small

clusters generally increase with decreasing cluster size, because there is less stabilization of the photoemission final state by screening and charge delocalization. Indeed, for smaller Pt_n, the Pt 4f BEs are shifted to higher BE compared to bulk Pt.[42, 50-53] Thus, the observation that $Pt_{24}/SiO_2/Si$ has a Pt 4f BE similar to that for bulk Pt, suggests that there must be some factor that offsets the expected final state shift to higher binding energy. The obvious factor is electron transfer from SiO_2/Si to Pt_{24}, which would tend to cause a shift to lower binding energy.

The sample with one ALD cycle shows only a small shift in the Pt binding energy. The Pt $4f_{7/2}$ peak in **Fig. 2** was fit to a BE of 71.1 eV, compared to 71.0 eV for the as-deposited sample. This 0.1 eV shift to higher binding energy can be compared to the much larger shifts observed for oxidized forms of bulk Pt (PtO ≈ 74.0 eV, PtO_2 ≈ 74.9 eV)[38], suggesting that the ALD overcoating process caused no change in Pt oxidation state. Therefore, the suppression of high temperature CO binding sites by ALD overcoating can be attributed to physical blocking of the Pt surface by Al_2O_3.

XP spectra give two, apparently contradictory measures of the alumina deposition rate in association with Pt clusters. Analysis of the Al 2p/Pt 4f ratio after a single ALD overcoating cycle shows that ~20 Al atoms deposit for every Pt atom on the surface – far more than would be expected for a self-limiting reaction. On the other hand, the attenuation of the Pt 4f signal by one cycle of ALD overlcoating is small, implying an alumina overlayer thickness of only ~3 Å, i.e., just about one alumina layer – far less than the 20:1 Al:Pt ratio implied by the peak intensities.

The implication is that the ALD process does, indeed, deposit approximately one alumina layer on top of the clusters, but in addition, the clusters seed alumina growth on the surrounding SiO_2/Si substrate. As noted above, ALD initiation on the vacuum-annealed SiO_2/Si substrate is quite inefficient, initially growing only ~5% of a monolayer/cycle. One contributing factor is

probably inefficient water dissociative adsorption on the vacuum-annealed SiO_2 surface, which has few reactive sites, as shown by the lack of 180 K CO adsorption on the substrates, for example. Therefore, one mechanism by which Pt clusters might catalyze growth on the surrounding substrate is water dissociative adsorption on the clusters, followed by spillover of H and/or OH to the substrate. Given the ~900 L water exposure used to initiate ALD, adsorption and spillover need not be efficient to substantially increase the number of substrate hydroxyl sites where TMA can react to initiate alumina growth.

A water TPD study on Pt(553) showed that H_2O does not adsorb on Pt(553) surface at 423 K and can only dissociate to OH when the surface is preadsorbed with atomic oxygen.[54] A recent XPS and theoretical study of H_2O adsorption on Pt nanoparticles also showed that H_2O weakly chemisorbs on Pt nanoparticles at room temperature.[55] These results would tend to suggest that the water dissociative spillover mechanism is not tenable, however, we are working with sub-nano Pt clusters, rather than bulk Pt or Pt nanoparticles. The Pt-Pt coordination in clusters is substantially smaller than even on the stepped (553) surface, thus the chemistry may be quite different. In addition, the fraction of sites at the cluster-substrate interface, and the distance that OH or H must diffuse to transition from cluster to substrate sites is much smaller than on nanoparticles.

The other mechanism by which Pt might catalyze alumina grown on the substrate would involve decomposition of TMA on the clusters, with spillover of Al-containing moieties to the SiO_2 substrate. Detwiler *et al.*[56] reported a study of TMA adsorption on Pt(111), where they found by XPS that TMA adsorbs on Pt (111) at 373 K. Density functional theory showed that TMA adsorbs dissociatively, with dissociation into monomethylaluminum and methyl being exothermic on Pt (111), while further dissociation to Al_{ads} + CH_{3ads} is only slightly endothermic.

Similar behavior was found for TMA on Pd (111) by Detwiler *et al.*[56] and Lu *et al.*[57, 58]. Lu *et al*. also reported that $AlCH_3$* can further dissociate into Al* and CH_3* on Pt(211) surfaces, and both $AlCH_3$ * and Al* transform into $Al(OH)_3$* species in the following H_2O exposure.[57] Thus, it is likely that TMA would adsorb dissociatively on Pt clusters, and the question is whether spillover of Al-containing species to the SiO_2 substrate is possible. Given the large TMA exposure used here, spillover would not need to be efficient in order to create a significant population of Al moieties on the substrate. Thus we conclude that spillover during either (or both) of the ALD reactant doses leading to alumina growth around the clusters is a reasonable mechanism to explain the large enhancement of Al deposition observed.

Here we observed that even the single alumina layer that deposits on top of the clusters is sufficient to completely block all Pt binding sites, and that even after repeated annealing cycles, only weak binding sites, become available. Recent work[10, 11] shows that CO binding sites associated with Au nanoparticles can be blocked by a TiO_2 ALD overcoat. DRIFTS CO chemisorption measurements showed that TiO_2 preferentially initiates at low-coordination sites on the Au nanoparticles and after 50 cycles of TiO_2 ALD, the peak intensity for adsorbed CO dropped by ~3 orders of magnitude. In our case, a single cycle of ALD is sufficient to block essentially all CO binding sites on our small Pt clusters, and after heating, only weak binding sites are exposed, with desorption temperatures below 200K.

For heterogeneous catalysis, different sites (terraces, edges) of nanoparticles are responsible for formation of different products during a catalytic reaction. Zhang et al.[4] previously reported that the selectivity of Pd nanoparticles (~1.3 nm) to furan, the product of furfural hydrogenation, increases after the Pd catalysts are overcoated with 10 cycles of alumina ALD. They concluded that terrace sites on Pd nanoparticles (which favor furan formation) remain

available after ALD, whereas step sites responsible for side reactions are passivated by the alumina. Using DRIFTS CO chemisorption, Feng et al.[2] also found that low-coordinated sites on Pd nanoparticles (~1.4 nm) are fully passivated by 8 cycles of alumina ALD. In our case, the Pt clusters are in an even smaller size range, with nearly all surface Pt atoms having low-coordination numbers, where ALD initiates with high efficiency, completely blocking all CO binding sites.

5. Conclusion

We have shown that alumina growth via ALD initiates with high efficiency on small Pt clusters on SiO_2/Si. The clusters were completely passivated by a single ALD cycle, and it was not possible to re-expose any strong Pt-associated CO binding sites by heating. We chose alumina ALD as a well characterized system for an initial study of ALD on sub-nanometer clusters. One conclusion if that if ALD initiates with high selectivity on small clusters, as is the case here, this could be an efficient approach to preparing size- and composition-selected bimetallic clusters for model catalysis studied, using size-selected clusters of one metal to seed selective deposition of a second metal by an ALD-like reaction sequence.

Acknowledgements

Funding: This work supported by the Air Force Office of Scientific Research under AFOSR grants FA9550-16-1-0141 and FA9550-19-1-0261. This research used resources of the Advanced Photon Source, a U.S. Department of Energy (DOE) Office of Science User Facility

operated for the DOE Office of Science by Argonne National Laboratory under Contract No. DE-AC02- 06CH11357.

References

[1] J.L. Lu, B.S. Fu, M.C. Kung, G.M. Xiao, J.W. Elam, H.H. Kung, P.C. Stair, Coking- and Sintering-Resistant Palladium Catalysts Achieved Through Atomic Layer Deposition, Science, 335 (2012) 1205-1208. http://doi.org/ 10.1126/science.1212906

[2] H. Feng, J. Lu, P.C. Stair, J.W. Elam, Alumina Over-coating on Pd Nanoparticle Catalysts by Atomic Layer Deposition: Enhanced Stability and Reactivity, Catal. Lett., 141 (2011) 512-517. https://doi.org/10.1007/s10562-011-0548-8

[3] B.J. O'Neill, D.H.K. Jackson, A.J. Crisci, C.A. Farberow, F. Shi, A.C. Alba-Rubio, J. Lu, P.J. Dietrich, X. Gu, C.L. Marshall, P.C. Stair, J.W. Elam, J.T. Miller, F.H. Ribeiro, P.M. Voyles, J. Greeley, M. Mavrikakis, S.L. Scott, T.F. Kuech, J.A. Dumesic, Stabilization of Copper Catalysts for Liquid-Phase Reactions by Atomic Layer Deposition, Angew. Chem. Int. Ed., 52 (2013) 13808-13812. https://doi.org/10.1002/anie.201308245

[4] H.B. Zhang, X.K. Gu, C. Canlas, A.J. Kropf, P. Aich, J.P. Greeley, J.W. Elam, R.J. Meyers, J.A. Dumesic, P.C. Stair, C.L. Marshall, Atomic Layer Deposition Overcoating: Tuning Catalyst Selectivity for Biomass Conversion, Angew. Chem. Int. Ed., 53 (2014) 12132-12136. https://doi.org/10.1002/anie.201407236

[5] B.J. O'Neill, D.H.K. Jackson, J. Lee, C. Canlas, P.C. Stair, C.L. Marshall, J.W. Elam, T.F. Kuech, J.A. Dumesic, G.W. Huber, Catalyst Design with Atomic Layer Deposition, ACS Catal., 5 (2015) 1804-1825. https://doi.org/10.1021/cs501862h

[6] M.M. Biener, J. Biener, A. Wichmann, A. Wittstock, T.F. Baumann, M. Bäumer, A.V. Hamza, ALD Functionalized Nanoporous Gold: Thermal Stability, Mechanical Properties, and Catalytic Activity, Nano Lett., 11 (2011) 3085-3090. https://doi.org/10.1021/nl200993g

[7] Z. Ma, S. Brown, J.Y. Howe, S.H. Overbury, S. Dai, Surface Modification of Au/TiO_2 Catalysts by SiO_2 via Atomic Layer Deposition, J. Phys. Chem. C., 112 (2008) 9448-9457. https://doi.org/10.1021/jp801484h

[8] J. Greeley, Structural Effects on Trends in the Deposition and Dissolution of Metal-supported Metal Adstructures, Electrochim. Acta, 55 (2010) 5545-5550. https://doi.org/10.1016/j.electacta.2010.04.055

[9] A.K. Rovik, S.K. Klitgaard, S. Dahl, C.H. Christensen, I. Chorkendorff, Effect of Alloying on Carbon Formation during Ethane Dehydrogenation, Appl. Catal. A., 358 (2009) 269-278. http://doi.org/10.1016/j.apcata.2009.02.020

[10] C. Wang, H. Wang, Q. Yao, H. Yan, J. Li, J. Lu, Precisely Applying TiO_2 Overcoat on Supported Au Catalysts Using Atomic Layer Deposition for Understanding the Reaction Mechanism and Improved Activity in CO Oxidation, J. Phys. Chem. C., 120 (2016) 478-486. https://doi.org/10.1021/acs.jpcc.5b11047

[11] Q. Yao, C. Wang, H. Wang, H. Yan, J. Lu, Revisiting the Au Particle Size Effect on TiO_2-Coated Au/TiO_2 Catalysts in CO Oxidation Reaction, J. Phys. Chem. C., 120 (2016) 9174-9183. https://doi.org/10.1021/acs.jpcc.5b12712

[12] C. Yin, F.R. Negreiros, G. Barcaro, A. Beniya, L. Sementa, E.C. Tyo, S. Bartling, K.-H. Meiwes-Broer, S. Seifert, H. Hirata, N. Isomura, S. Nigam, C. Majumder, Y. Watanabe, A. Fortunelli, S. Vajda, Alumina-supported Sub-nanometer Pt_{10} Clusters: Amorphization and Role of the Support Material in a Highly Active CO Oxidation Catalyst, J. Phys. Chem. A., (2017). http://doi.org/10.1039/C6TA10989F

[13] R.E. Winans, S. Vajda, G.E. Ballentine, J.W. Elam, B. Lee, M.J. Pellin, S. Seifert, G.Y. Tikhonov, N.A. Tomczyk, Reactivity of Supported Platinum Nanoclusters Studied by in situ GISAXS: Clusters Stability under Hydrogen, Top. Catal., 39 (2006) 145-149. https://doi.org/10.1007/s11244-006-0050-5

[14] S. Lee, B. Lee, F. Mehmood, S. Seifert, J.A. Libera, J.W. Elam, J. Greeley, P. Zapol, L.A. Curtiss, M.J. Pellin, P.C. Stair, R.E. Winans, S. Vajda, Oxidative Decomposition of Methanol on Subnanometer Palladium Clusters: The Effect of Catalyst Size and Support Composition, J. Phys. Chem. C., 114 (2010) 10342-10348. https://doi.org/10.1021/jp912220w

[15] S. Vajda, M.J. Pellin, J.P. Greeley, C.L. Marshall, L.A. Curtiss, G.A. Ballentine, J.W. Elam, S. Catillon-Mucherie, P.C. Redfern, F. Mehmood, P. Zapol, Subnanometre Platinum Clusters as Highly Active and Selective Catalysts for the Oxidative Dehydrogenation of Propane, Nat. Mater., 8 (2009) 213-216.httP://doi.org/ 10.1038/nmat2384

[16] S. Lee, M. Molina Luis, J. Lopez Maria, A. Alonso Julio, B. Hammer, B. Lee, S. Seifert, E. Winans Randall, W. Elam Jeffrey, J. Pellin Michael, S. Vajda, Selective Propene Epoxidation on Immobilized $Au_{(6-10)}$ Clusters: the Effect of Hydrogen and Water on Activity and Selectivity, Angew Chem Int Ed Engl, 48 (2009) 1467-1471. http://doi.org/ 10.1002/anie.200804154

[17] Y. Dai, T.J. Gorey, S.L. Anderson, S. Lee, S. Lee, S. Seifert, R.E. Winans, Inherent Size Effects on XANES of Nanometer Metal Clusters: Size-Selected Platinum Clusters on Silica, J. Phys. Chem. C., 121 (2017) 361-374. https://doi.org/10.1021/acs.jpcc.6b10167

[18] M.-A. Ha, E.T. Baxter, A.C. Cass, S. L.Anderson, A.N. Alexandrova, Boron Switch for Selectivity of Catalytic Dehydrogenation on Size-Selected Pt clusters on Al_2O_3, J. Am. Chem. Soc., 139 (2017) 11568-11575. https://doi.org/10.1021/jacs.7b05894

[19] E.T. Baxter, M.-A. Ha, A.C. Cass, H. Zhai, A.N. Alexandrova, S.L. Anderson, Diborane Interactions with Pt_7/alumina: Preparation of Size-Controlled Boronated Pt Model Catalysts with Improved Coking Resistance, J. Phys. Chem. C., 122 (2018) 1631-1644. https://doi.org/10.1021/acs.jpcc.7b10423

[20] T.J. Gorey, B. Zandkarimi, G. Li, E.T. Baxter, A.N. Alexandrova, S.L. Anderson, Preparation of Size and Composition Controlled Pt_nSn_x/SiO_2 (n = 4, 7, 24) Bimetallic Model Catalysts with Atomic Layer Deposition, J. Phys. Chem. C., 123 (2019) 16194-16209. https://doi.org/10.1021/acs.jpcc.9b02745

[21] A.W. Ott, J.W. Klaus, J.M. Johnson, S.M. George, Al_2O_3 Thin Film Growth on Si(100) using Binary Reaction Sequence Chemistry, Thin Solid Films, 292 (1997) 135-144. http://doi.org/10.1016/S0040-6090(96)08934-1

[22] C. Jiao, C. A. DeJoseph Jr, P. Haaland, A. Garscadden, Electron Impact Ionization and Ion Chemistry in Trimethylaluminum and in Trimethylgallium, Int. J. Mass. Spectrom., 202 (2000) 345-349. https://doi.org/10.1016/S1387-3806(00)00258-X

[23] W. Hwang, Y.K. Kim, M.E. Rudd, New Model for Electron-impact Ionization Cross Sections of Molecules, J. Chem. Phys., 104 (1996) 2956-2966. https://doi.org/10.1063/1.471116

[24] W.E. Kaden, W.A. Kunkel, S.L. Anderson, Cluster Size Effects on Sintering, CO Adsorption, and Implantation in Ir/SiO_2, J. Chem. Phys., 131 (2009) 114701, 114701-114715. https://doi.org/10.1063/1.3224119

[25] M. Aizawa, S. Lee, S.L. Anderson, Deposition Dynamics and Chemical Properties of Size-selected Ir Clusters on TiO_2, Surf. Sci., 542 (2003) 253-275. https://doi.org/10.1016/S0039-6028(03)00984-1

[26] W.E. Kaden, W.A. Kunkel, F.S. Roberts, M. Kane, S.L. Anderson, CO Adsorption and Desorption on Size-selected $Pd_n/TiO_2(110)$ Model Catalysts: Size Dependence of Binding Sites and Energies, and Support-mediated Adsorption, J. Chem. Phys., 136 (2012) 204705/204701-204705/204712. https://doi.org/10.1063/1.4721625

[27] S. Lee, B. Lee, S. Seifert, S. Vajda, R.E. Winans, Simultaneous Measurement of X-ray Small Angle Scattering, Absorption and Reactivity: A Continuous Flow Catalysis Reactor, Nucl. Instrum. Methods Phys. Res., Sect. A., 649 (2011) 200-203. https://doi.org/10.1016/j.nima.2010.12.172

[28] J. Ilavsky, P.R. Jemian, Irena: Tool Suite for Modeling and Analysis of Small-angle Scattering, J. Appl. Crystallogr., 42 (2009) 347-353. https://doi.org/10.1107/S0021889809002222

[29] J.J. Yeh, I. Lindau, Atomic Subshell Photoionization Cross Sections and Asymmetry Parameters: 1< Z < 103, Atomic Data and Nuclear Data Tables, 32 (1985) 1-155.

[30] C.J. Powell, A. Jablonski, NIST Electron Effective-Attenuation-Length Database v. 1.1, 1.1 ed., NIST, Gaithersburg, MD, 2003.

[31] R.A. Wind, S.M. George, Quartz Crystal Microbalance Studies of Al_2O_3 Atomic Layer Deposition using Trimethylaluminum and Water at 125 degrees C, J. Phys. Chem. A., 114 (2010) 1281-1289. http://doi.org/10.1021/jp9049268

[32] J.W. Elam, M.D. Groner, S.M. George, Viscous Flow Reactor with Quartz Crystal Microbalance for Thin Film Growth by Atomic Layer Deposition, Rev. Sci. Instrum., 73 (2002) 2981-2987. https://doi.org/10.1063/1.1490410

[33] M.D. Groner, F.H. Fabreguette, J.W. Elam, S.M. George, Low-Temperature Al_2O_3 Atomic Layer Deposition, Chem. Mater., 16 (2004) 639-645. https://doi.org/10.1021/cm0304546

[34] M.D. Groner, J.W. Elam, F.H. Fabreguette, S.M. George, Electrical Characterization of Thin Al_2O_3 Films Grown by Atomic Layer Deposition on Silicon and Various Metal Substrates, Thin Solid Films, 413 (2002) 186-197. https://doi.org/10.1016/S0040-6090(02)00438-8

[35] J.M. Lownsbury, J.A. Gladden, C.T. Campbell, I.S. Kim, A.B.F. Martinson, Direct Measurements of Half-Cycle Reaction Heats during Atomic Layer Deposition by Calorimetry, Chem.Mater., 29 (2017) 8566-8577. https://doi.org/10.1021/acs.chemmater.7b01491

[36] R. Matero, A. Rahtu, M. Ritala, M. Leskelä, T. Sajavaara, Effect of Water Dose on the Atomic Layer Deposition Rate of Oxide Thin Films, Thin Solid Films, 368 (2000) 1-7. https://doi.org/10.1016/S0040-6090(00)00890-7

[37] K. Kukli, M. Ritala, M. Leskelä, J. Jokinen, Atomic Layer Epitaxy Growth of Aluminum Oxide Thin Films from a Novel $Al(CH_3)_2Cl$ Precursor and H_2O, J. Vac. Sci. Technol. A, 15 (1997) 2214-2218. https://doi.org/10.1116/1.580536

[38] C.D. Wagner, A.V. Naumkin, A. Kraut-Vass, J.W. Allison, C.J. Powell, J.R.R. Jr., NIST X-ray Photoelectron Spectroscopy Database, NIST Standard Reference Database 20, Version 3.2 (Web Version), (2000).

[39] D.R. Strongin, J.F. Moore, M.W. Ruckman, Synchrotron Radiation Assisted Deposition of Aluminum Oxide from Condensed Layers of Trimethylaluminum and Water at 78 K, Appl. Phys. Lett., 61 (1992) 729-731. https://doi.org/10.1063/1.107781

[40] R.E. Winans, S. Vajda, B. Lee, S.J. Riley, S. Seifert, G.Y. Tikhonov, N.A. Tomczyk, Thermal Stability of Supported Platinum Clusters Studied by in Situ GISAXS, J. Phys. Chem. B., 108 (2004) 18105-18107. https://doi.org/10.1021/jp045549p

[41] J.W. Rabalais, Principles and Applications of Ion Scattering Spectrometry : Surface Chemical and Structural Analysis, Wiley, New York, 2003.

[42] F.S. Roberts, M.D. Kane, E.T. Baxter, S.L. Anderson, Oxygen Activation and CO Oxidation over Size-selected Pt_n/alumina/Re(0001) Model Catalysts: Correlations with Valence Electronic Structure, Physical Structure, and Binding Sites, Phys. Chem. Chem. Phys., 16 (2014) 26443 – 26457. https://doi.org/10.1039/C4CP02083A

[43] E. Baxter, T., M.-A. Ha, A. Alexandrova, S.L. Anderson, Ethylene Dehydrogenation on $Pt_{4,7,8}$ Clusters on Al_2O_3: Strong Cluster-Size Dependence Linked to Preferred Catalyst Morphologies, ACS Catal., 7 (2017) 3322-3335. https://doi.org/10.1021/acscatal.7b00409

[44] P.A. Redhead, Thermal Desorption of Gases, Vacuum, 12 (1962) 203-211. https://doi.org/10.1016/0042-207X(62)90978-8

[45] M.D. Kane, F.S. Roberts, S.L. Anderson, Alumina Support and Pd_n Cluster Size Effects on Activity of Pd_n for Catalytic Oxidation of CO, Faraday Discuss., 162 (2013) 323 - 340. https://doi.org/10.1039/c3fd20151a

[46] M.D. Kane, F.S. Roberts, S.L. Anderson, Effects of Alumina Thickness on CO Oxidation Activity over Pd_{20}/Alumina/Re(0001): Correlated Effects of Alumina Electronic Properties and Pd_{20} Geometry on Activity, J. Phys. Chem. C., 119 (2015) 1359–1375. https://doi.org/10.1021/jp5093543

[47] T.R. Gow, R. Lin, L.A. Cadwell, F. Lee, A.L. Backman, R.I. Masel, Decomposition of Trimethylaluminum on Silicon(100), Chem. Mater., 1 (1989) 406-411. https://doi.org/10.1021/cm00004a006

[48] C.C. Chusuei, X. Lai, K. Luo, D.W. Goodman, Modeling Heterogeneous Catalysts: Metal Clusters on Planar Oxide Supports, Top. Catal., 14 (2001) 71-83. https://doi.org/10.1023/A:1009059100646

[49] P.S. Bagus, Chemical Information from XPS Binding Energy Shifts: A Unified View, Abstracts of Papers, 225th ACS National Meeting, New Orleans, LA, United States, March 23-27, 2003, (2003) COLL-446.

[50] W.E. Kaden, T. Wu, W.A. Kunkel, S.L. Anderson, Electronic Structure Controls Reactivity of Size-Selected Pd Clusters Adsorbed on TiO_2 Surfaces, Science, 326 (2009) 826-829. https://doi.org/10.1126/science.1180297

[51] W.E. Kaden, C. Büchner, L. Lichtenstein, S. Stuckenholz, F. Ringleb, M. Heyde, M. Sterrer, H.-J. Freund, L. Giordano, G. Pacchioni, C.J. Nelin, P.S. Bagus, Understanding Surface Core-Level Shifts using the Auger Parameter; a study of Pd atoms adsorbed on SiO_2 Ultra-thin Films, Phys. Rev. B, 89 (2014) 115436 115431-115438. DOI:10.1103/PhysRevB.89.115436

[52] F.S. Roberts, S.L. Anderson, A.C. Reber, S.N. Khanna, Initial and Final State Effects in the Ultraviolet and X-ray Photoelectron Spectroscopy (UPS and XPS) of Size-Selected Pd_n Clusters Supported on TiO_2(110), J. Phys. Chem. C., 119 (2015) 6033-6046. https://doi.org/10.1021/jp512263w

[53] M.D. Kane, F.S. Roberts, S.L. Anderson, Mass-selected Supported Cluster Catalysts: Size Effects on CO Oxidation Activity, Electronic Structure, and Thermal Stability of Pd_n/alumina ($n \leq 30$) Model Catalysts, Int. J. Mass Spectrom., 370 (2014) 1-15. https://doi.org/10.1016/j.ijms.2014.06.018

[54] M.J.T.C. van der Niet, A. den Dunnen, L.B.F. Juurlink, M.T.M. Koper, A Detailed TPD Study of H_2O and Pre-adsorbed O on the Stepped Pt(553) Surface, Phys. Chem. Chem. Phys., 13 (2011) 1629-1638. https://doi.org/10.1039/C0CP01162B

[55] Y. Cui, Y. Harada, E. Ikenaga, R. Li, N. Nakamura, T. Hatanaka, M. Ando, T. Yoshida, G.-L. Li, M. Oshima, In Situ Hard X-ray Photoelectron Study of O_2 and H_2O Adsorption on Pt Nanoparticles, J. Phys. Chem. C., 120 (2016) 10936-10940. https://doi.org/10.1021/acs.jpcc.6b02402

[56] M.D. Detwiler, A. Gharachorlou, L. Mayr, X.K. Gu, B. Liu, J. Greeley, W.N. Delgass, F.H. Ribeiro, D.Y. Zemlyanov, Reaction of Trimethylaluminum with Water on Pt(111) and Pd(111) from 10^{-5} to 10^{-1} Millibar, J. Phys. Chem C., 119 (2015) 2399-2411. https://doi.org/10.1021/jp510032u

[57] J.L. Lu, B. Liu, N.P. Guisinger, P.C. Stair, J.P. Greeley, J.W. Elam, First-Principles Predictions and in Situ Experimental Validation of Alumina Atomic Layer Deposition on Metal Surfaces, Chem. of Mater., 26 (2014) 6752-6761. https://doi.org/10.1021/cm503178j

[58] J. Lu, B. Liu, J.P. Greeley, Z. Feng, J.A. Libera, Y. Lei, M.J. Bedzyk, P.C. Stair, J.W. Elam, Porous Alumina Protective Coatings on Palladium Nanoparticles by Self-Poisoned Atomic Layer Deposition, Chem. Mater, 24 (2012) 2047-2055. https://doi.org/10.1021/cm300203s

Selective Growth of Al_2O_3 on Size-Selected Platinum Clusters by Atomic Layer Deposition

Timothy J. Gorey,[a] *Yang Dai,*[a] *Scott L. Anderson*[1a*]

Sungsik Lee[1b], *Sungwon Lee,*[b] *Soenke Seifert*[b] *and Randall E. Winans*[b]

[a]Chemistry Department, University of Utah, Salt Lake City, UT 84112

[b]X-ray Science Division, Argonne National Laboratory, 9700 South Cass Ave, Argonne, IL 60439

[1] Senior Author and Corresponding Author: anderson@utah.edu

SUPPORTING INFORMATION

Al_2O_3 Growth Rate on SiO_2 with Larger Doses of H_2O+TMA

To test whether the Al_2O_3 growth on SiO_2 is a self-limiting deposition, the dose of water and trimethylaluminum (TMA) was increased to 5.0 x 10^{-5} Torr for 150s (25x higher than the doses used in **Fig. 1**). All other experimental parameters, such as the SiO_2 wafer cleaning procedure and 423 K sample temperature were kept constant relative to that shown in **Fig. 1**. The results are shown in **Fig. S1**. The top panel shows the Al 2p region, with the raw data (symbols) fit with a Gaussian-Lorentzian line shape. Clearly, the amount of Al_2O_3 on the SiO_2 increases with more cycles, and as seen in **Fig. 1**, the amount of Al_2O_3 deposited per cycle increases as more cycles are performed. Using the integrated intensities obtained from the fits, overlayer thicknesses were calculated using the model described in the main text with respect to **Fig. 1**. The overlayer thickness was plotted in the lower panel as a function of ALD cycle number. Results show that the higher exposure over the course of 12 cycles results in ~ 0.4 Å of Al_2O_3 deposited per cycle. The normal dose used in most experiments is 2.0 x 10^{-6} Torr for 150 s. Shown in **Fig. 1**, the lower dose also resulted in a growth rate of ~0.4 Å per cycle over the course of 12

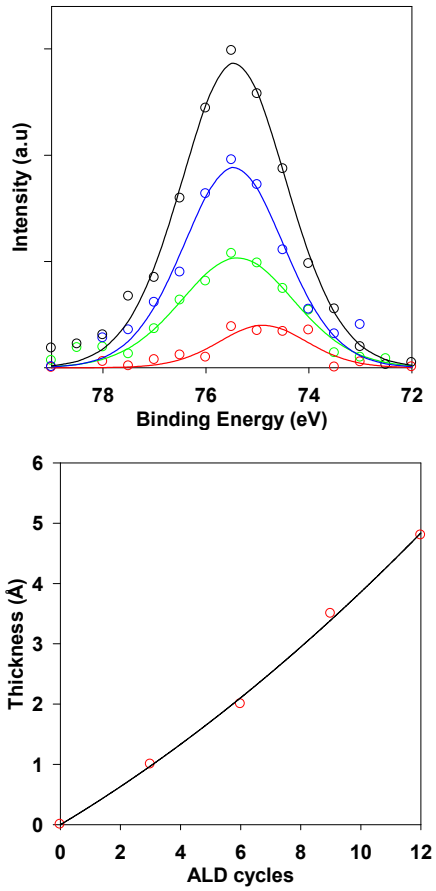

Fig. S1. The growth rate calibration of alumina ALD on clean SiO_2/Si (100) at the surface temperature of 423 K. Dose pressures for H_2O and TMA were increased to 5 x 10^{-5} Torr. Calculated thickness of Al_2O_3 is shown as a function of ALD cycles.

ALD cycles. If the reaction is self-limiting, i.e. the amount of Al_2O_3 deposited to the SiO_2 surface is limited by the number of nucleation sites, then increased exposure well above the saturation dose would result in no additional Al_2O_3. Indeed this is the case here, providing evidence of an ALD reaction limited by the number of nucleation sites on the surface.

Al_2O_3 ALD Growth Rate on SiO_2 at 300 K

To test the temperature dependence on ALD growth rate, similar ALD growth rate experiments to that shown in **Fig. 1**, were conducted at a sample temperature of 300 K. In this case, all other experimental parameters, such as the SiO_2 crystal preparation and H_2O/TMA exposures were done as described for that in **Fig. 1**. Results for Al_2O_3 ALD done for a sample temperature of 300 K are shown in **Fig. S2**. As before the raw XPS intensities for the Al 2p were fit with Gaussian-Lorentzian line shapes, and the integrated values were used to calculate the overlayer thickness using the XPS intensity from the O 1s (from the 1.1 nm oxide film) as a reference. The 300 K ALD deposition resulted in 0.92 Å Al_2O_3 being deposited per cycle, which is ~56% more efficient than that done at 423 K. The higher deposition rate is likely a result of more nucleation sites (surface hydroxyls) being available on SiO_2 at room temperature. Heating to 423 K likely desorbs –OH groups on the surface that normally would react and anchor the TMA molecules.

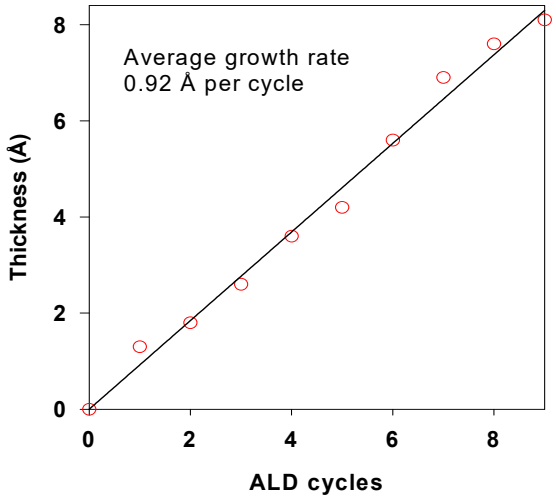

Fig. S2. The growth rate calibration of alumina ALD on clean SiO_2/Si (100) at the surface temperature of 300 K. Calculated thickness of Al_2O_3 is shown as a function of ALD cycles.

Full ISS Survey Spectrum of Pt_{24}/SiO_2

A sample ISS spectrum was collected. 0.1 ML Pt_{24} was soft-landed onto a clean SiO_2 wafer, and the as-deposited sample was transferred to the *in situ* spectroscopy chamber. A single ISS survey scan was collected for the entire energy range using 3.0 μA of 1 keV He^+. The final kinetic energy of scattered ions, as measured by the spectrometer, was divided by the incident He^+ beam energy giving E/E_0. The spectrum is shown in **Fig. S3**. Peaks for oxygen, silicon, and platinum are clearly present at 0.40, 0.58, and 0.93 E/E_0 respectively. Note that the analysis area for the hemispherical spectrometer used in this spectrum is larger than the cluster spot, thus the intensities for silicon and oxygen are artificially high relative to Pt. Since our primary interest is in changes induced in the Pt peak by overlayers or adsorbates, this area mismatch has no effect on the analysis.

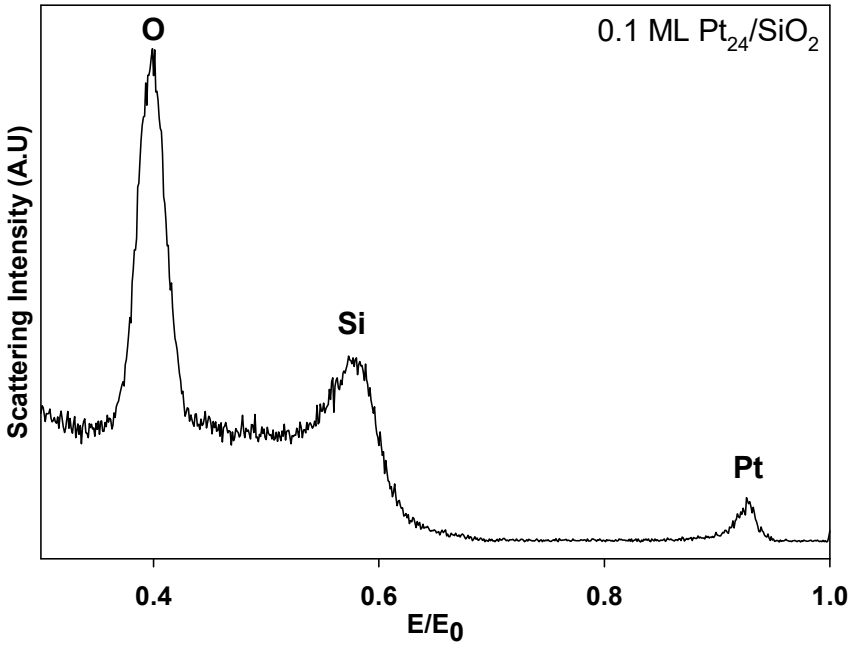

Fig. S3. Full energy range ISS scan of as-deposited Pt_{24}/SiO_2.

Mass 16 Desorption from 1 ALD Overcoated Pt_{24}/SiO_2 (300 K vs 423 K)

To measure the removal of organic molecules from the surface, mass 16 (CH_4^+) was monitored during sequential heat ramps applied to 1 ALD overcoated Pt_{24}/SiO_2. 0.1 ML of Pt_{24} clusters were deposited onto a clean SiO_2 wafer then exposed to 150 seconds of 2 x 10^{-6} Torr

H_2O, followed by 150 seconds of 2 x 10^{-6} Torr TMA, and a final 5 min of 2 x 10^{-6} Torr H_2O exposure. The resulting sample was moved to the TPD stage and heated linearly at 3 K/s to 600 K from a starting temperature of 280 K. The mass 16 desorption from the ALD deposited at 300 K is shown in **Fig. S3 (top)**, and that for 423 K is shown in **Fig S3 (bottom)**. Desorption begins around the temperature ALD was performed at, which is expected as molecules occupying binding sites below the ALD temperature would spontaneously desorb. For both samples, mass 16 desorption continues above 500 K, but reaches a maximum before completion of the heat ramp. In sequential thermal desorption spectra, no additional mass 16 desorption is detected, indicating that all material within that temperature range has desorbed. Note that the mass 16 desorption does not completely cease to baseline within this temperature range; this suggests that additional strongly bound organic material could remain on the surface.

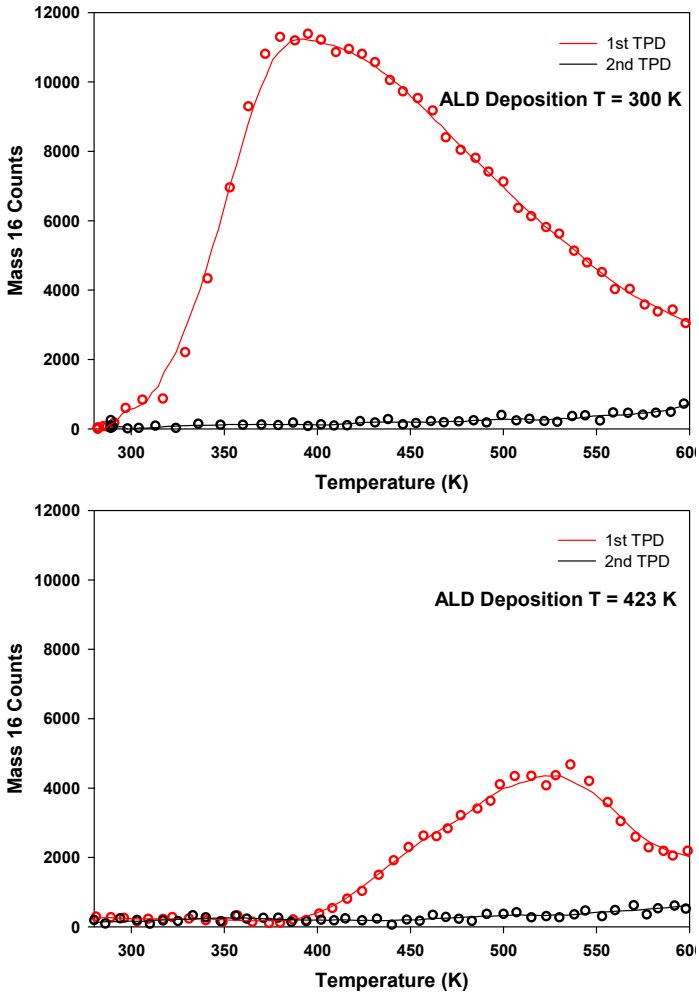

Fig. S4. Sequential thermal desorption spectra of mass 16 from 1 ALD/Pt_{24}/SiO_2/Si, with ALD deposited at 300 K (top) and 423 K (bottom).